Nuclear Inst. and Methods in Physics Research, A 878 (2018) 159–168

Contents lists available at ScienceDirect

Nuclear Inst. and Methods in Physics Research, A

journal homepage: www.elsevier.com/locate/nima

Gamma-Ray imaging for nuclear security and safety: Towards 3-D gamma-ray vision

Kai Vetter [a,b,*], Ross Barnowksi [b], Andrew Haefner [b], Tenzing H.Y. Joshi [b], Ryan Pavlovsky [a], Brian J. Quiter [b]

[a] Department of Nuclear Engineering, University of California Berkeley, Berkeley, CA 94720, USA
[b] Nuclear Science Division, Lawrence Berkeley National Laboratory, Berkeley, CA, 94720, USA

ARTICLE INFO

Keywords:
Gamma-ray imaging
Multi-modality imaging
Data fusion
Radiation detection
Gamma-ray vision

ABSTRACT

The development of portable gamma-ray imaging instruments in combination with the recent advances in sensor and related computer vision technologies enable unprecedented capabilities in the detection, localization, and mapping of radiological and nuclear materials in complex environments relevant for nuclear security and safety. Though multi-modal imaging has been established in medicine and biomedical imaging for some time, the potential of multi-modal data fusion for radiological localization and mapping problems in complex indoor and outdoor environments remains to be explored in detail. In contrast to the well-defined settings in medical or biological imaging associated with small field-of-view and well-constrained extension of the radiation field, in many radiological search and mapping scenarios, the radiation fields are not constrained and objects and sources are not necessarily known prior to the measurement. The ability to fuse radiological with contextual or scene data in three dimensions, in analog to radiological and functional imaging with anatomical fusion in medicine, provides new capabilities enhancing image clarity, context, quantitative estimates, and visualization of the data products. We have developed new means to register and fuse gamma-ray imaging with contextual data from portable or moving platforms. These developments enhance detection and mapping capabilities as well as provide unprecedented visualization of complex radiation fields, moving us one step closer to the realization of gamma-ray vision in three dimensions.

Contents

1. Introduction

Gamma-ray imaging is well established in many fields, including medicine, biomedical research, and astrophysics. It also has found applications in nuclear security and safety providing means to detect, localize, and characterize nuclear materials in a range of uses and environments. Of general concern for security is the misuse of radioactive materials as utilized in industrial and medical applications. Of particular concern is the safeguarding and proliferation of so-called Special Nuclear Materials (SNM), such as enriched ^{235}U or ^{239}Pu, and

* Corresponding author at: Department of Nuclear Engineering, University of California Berkeley, Berkeley, CA 94720, USA.
E-mail address: kvetter@berkeley.edu (K. Vetter).

http://dx.doi.org/10.1016/j.nima.2017.08.040
Received 8 May 2017; Received in revised form 7 August 2017; Accepted 22 August 2017
Available online 8 September 2017

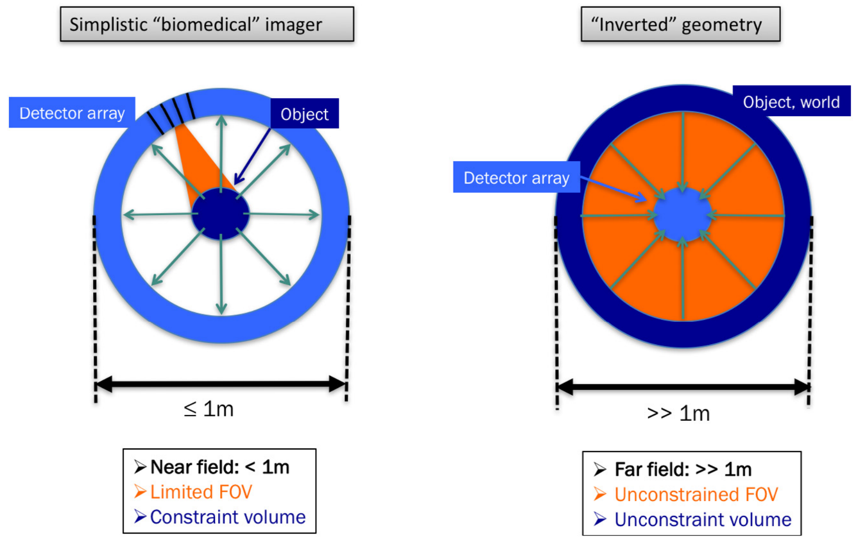

Fig. 1. Illustration of concepts and domains for gamma-ray imaging in "classical" biomedical imaging (left) and nuclear security and safety (right). Green arrows indicate the direction of gamma rays. In biomedical imaging, the object is restricted to a constrained FOV and the radiation source is restricted to a known and constrained volume that can be observed from many angles, always in a well-described geometry and path. In contrast, in nuclear security, the FOV and imaging volume can be unrestricted and only limited projections can be obtained. (For interpretation of the references to color in this figure legend, the reader is referred to the web version of this article.)

associated operations as well as the prevention of proliferation and illicit use of SNM internationally and domestically. The characteristic gamma-ray emission lines of these isotopes, and their decay daughters, serve as fingerprints to identify specific isotopes and their decay daughters. For applications related to radiological safety, gamma-ray imaging provides powerful means to detect and map leaks, lost sources, or contamination after nature- or man-induced accidents. Though in principle the objectives of gamma-ray imaging in the diverse fields mentioned above are similar, the contexts and domains are quite different, and require different implementations. Fig. 1 attempts to capture the main conceptual differences between medical imaging and imaging in nuclear security and safety. In biomedical imaging, the imaging object is well-constrained in space allowing a gamma-ray imager to be built around the object or to move in a well-defined path around the object such that the system may be designed to limit the field of view (FOV) for each detector to the imaged object. In nuclear security and safety or more broadly, in environmental imaging, the object is not necessarily constrained in space and the relationship between imaging system and image object are spatially inverted. In addition, since the measurements path is not fixed requiring a freely moving system, the location and orientation of the imaging instrument needs to be determined and tracked relative to the surrounding objects, or world.

Furthermore, the enormous gain in fusing different and complementary imaging modalities was recognized in medicine and biomedical imaging a long time ago, however, data fusion is not yet widely utilized in security and safety. For example, in medical, biomedical, or biological imaging, X-ray imaging is combined with gamma-ray imaging fusing anatomical and functional features in a high-dimensional image. In contrast, in the utilization of gamma-ray imaging for safety and security, to-date only static and two-dimensional gamma-ray image projections are overlaid with two-dimensional visual images, as indicated in Fig. 2 [1–14].

Recent advances in sensor technologies such as structured light or LiDAR now enable the full integration and fusion of "anatomical" or contextual and "functional" or gamma-ray imaging data in the less constrained security, safety, and environmental domain. In the following, we will briefly discuss the underlying concept of what we call scene-data fusion (SDF) followed by instruments we have successfully utilized to develop and demonstrate this concept. Results of measurements are split between ground-based and aerial deployments reflecting the wide range of applications for this new concept.

2. Scene-data fusion

The concept of scene-data fusion is based on the integration of contextual scene data with – in the broadest sense – any type of emission data in three dimensions [15–17]. The contextual scene data is obtained by sensors, such as visual cameras, structured light, or LiDAR that enable the reconstruction or mapping of a scene in 3-D. This scene or map is then used to determine the position and orientation (i.e. the pose) of the instrument in this scene, which is registering emissions from the scene constituents. We use Simultaneous Location and Mapping (SLAM) algorithms to achieve the mapping of the scene and tracking of the pose of the instrument [18]. SLAM is being used to create and update the scene map while simultaneously providing the six-dimensional information about location and orientation of the sensor within this scene map. It is widely being used in robotics tracking and navigation. The goal here is not to describe the details of the specific and publicly available SLAM algorithms, which we are employing but the fact that these algorithms can provide the critical information for the mapping, pose estimation, and ultimately the realization of 3-D SDF. In general, the output of the SLAM algorithm are point clouds representing the coordinates of object surfaces relative to the instrument.

While any emission data such as infrared or hyperspectral or radiation of nuclear origin such as gamma rays and neutrons can be used in SDF, our focus here is on gamma rays. Gamma rays provide powerful fingerprints for detecting and identifying specific radioisotopes, assuming the instrument is implemented as spectrometer, i.e. able to measure the energies of the gamma rays. The identification can be done for radioisotopes with known gamma-ray energies or the energies can be used to identify the radioisotope that is being observed.

Detecting the full energy of an incident gamma ray implies that the gamma ray did not scatter between the source and the detector and therefore, maintained the direction to the source. In addition, the number of counts in the full-energy or photo-peak can be associated with the amount or mass of the emitting source, assuming the absorbing material between source detector can be neglected, is known, or can be otherwise obtained. SDF does provide the information about the distance between the source and the detector at any moment of the measurement enabling the possibility to estimate of the source strength. The estimation of specific quantification is currently under development and not included here.

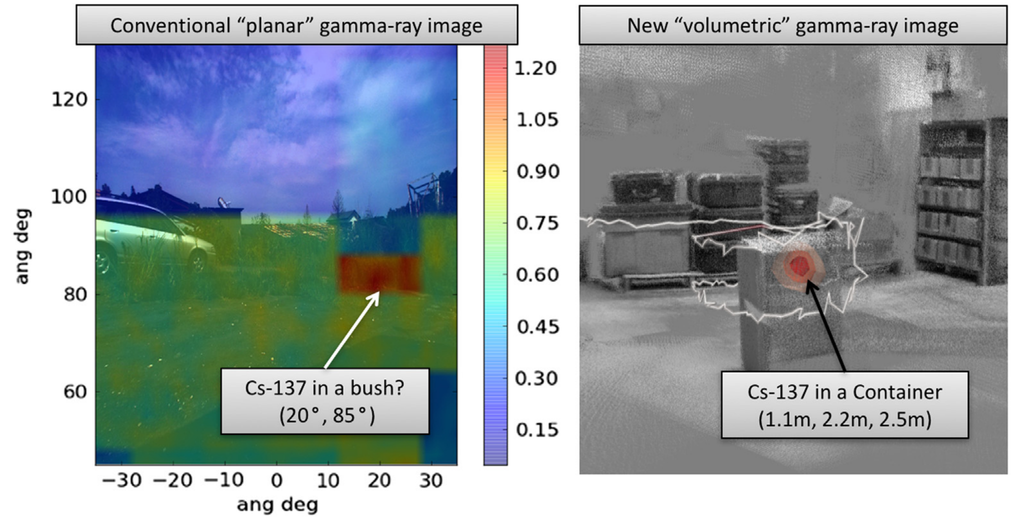

Fig. 2. Illustration of current approach of "planar" gamma-ray imaging with gamma-ray visual overlay in two dimensions (left) and new "volumetric" gamma-ray imaging or scene-data fusion based on full fusion of contextual and gamma-ray image data in three dimensions. The three coordinates represent the location of the detected source in the container with regard to an arbitrary but fixed coordinate system provided by the localization and mapping algorithms utilized.

Fig. 3 illustrates SDF by showing a reconstructed scene from moving an instrument through our laboratory. In this specific case, a position-sensitive HPGe detector was operated in Compton imaging mode in combination with a Microsoft Kinect sensor. SLAM enables the mapping of the scene and the estimation of the pose and tracking of the instrument in the scene as reflected by the red line. The white spheres indicate individual 662 keV gamma-ray events that were used to reconstruct the location of a ^{137}Cs point source. The location of the 50 μCi point source is indicated by the red arrow. The instrument was moved slowly along a slightly curved path of 4.6 m with a minimum distance of 1.5 m between it and the source. In the 124 s duration of this measurement, 85 full-energy Compton events were collected and utilized for the reconstruction. The specific gamma-ray imaging instrument and imaging modality is being discussed below. The point cloud of the reconstructed scene in combination with a Maximum Likelihood Expectation Maximization (MLEM) algorithm was used for the gamma-ray image reconstruction. Specifically, list-mode MLEM is being deployed to make the reconstruction tractable for three-dimensional Compton image reconstruction. One approach to make use of the point cloud information is to only use voxels for the image reconstruction that contain at least one point of the point cloud. In Compton imaging, cones are created whose extension represents all possible incident angles of a specific gamma ray [19–25]. The expectation maximization of the algorithms maximizes the likelihood of the source location over many gamma rays given the underlying statistical Poisson characteristics. In the list-mode implementation, sensitivities are computed given the distances between the instrument and a specific image voxel and the system matrix is computed using the three-dimensional cone with an intrinsic Gaussian width and its overlap with the voxels in image space. Each voxel is also represented by a Gaussian shape in three dimension with a specific width. The cone width is typically 10° reflecting the angular resolution of the employed gamma-ray imagers, the extension of the image voxel is typically 10 cm in all three dimensions. The latter can be adjusted according to distances between objects and the instrument or to optimize computing speed [4,15,16,26,27]. The imaging algorithm runs in near real-time: a non-optimized, implementation takes 200 ms to compute the backprojection and another 200 ms to complete 10 iterations on a single core (no multithreading) of an Intel i7 4600U at 2.1 GHz. The computing time strongly depends on the dimension and complexity of the scene. The number of iterations was chosen to balance the real-time requirement with image convergence, with 10 being empirically determined to be sufficient for the reconstruction of point sources.

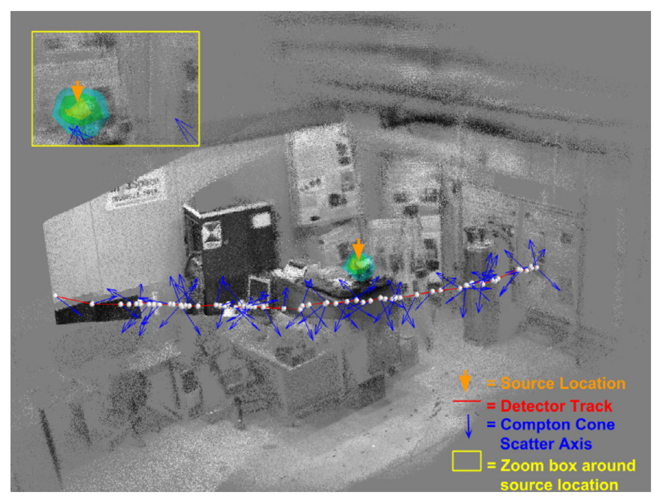

Fig. 3. Illustration of SDF. A double-sided strip detector (DSSD) made of high-purity germanium (HPGe) was used in combination with a Microsoft Kinect sensor attached to the gamma-ray detector. The red line is the reconstructed path in the scene, the white spheres indicate the location of the gamma-ray events used in the image reconstruction, the blue arrows show the scattering direction of the Compton gamma rays within the detector, and the orange arrow shows the true location of the ^{137}Cs source in 3-D. The inset magnifies the position of the detected, identified, and localized source. (For interpretation of the references to color in this figure legend, the reader is referred to the web version of this article.)

The fact that the reconstructed point cloud can be used for the image reconstruction provides a powerful advantage of SDF over conventional gamma-ray imaging approaches as the reconstruction space can be significantly reduced providing much higher processing speed and improved accuracy and less noise in the reconstruction. In the example of Fig. 3, 2.8×10^4 voxels are being used when the image space is constrained by the point cloud as compared with $1.6{\times}10^6$ voxels without this constraint.

3. Instruments

Several instruments have been built or enhanced to enable SDF. Fig. 4 shows the High-Efficiency Multimode Imager (HEMI) that was augmented with a Microsoft Kinect sensor [28]. HEMI is a hand-portable gamma-ray imager that provides coded aperture and Compton imaging

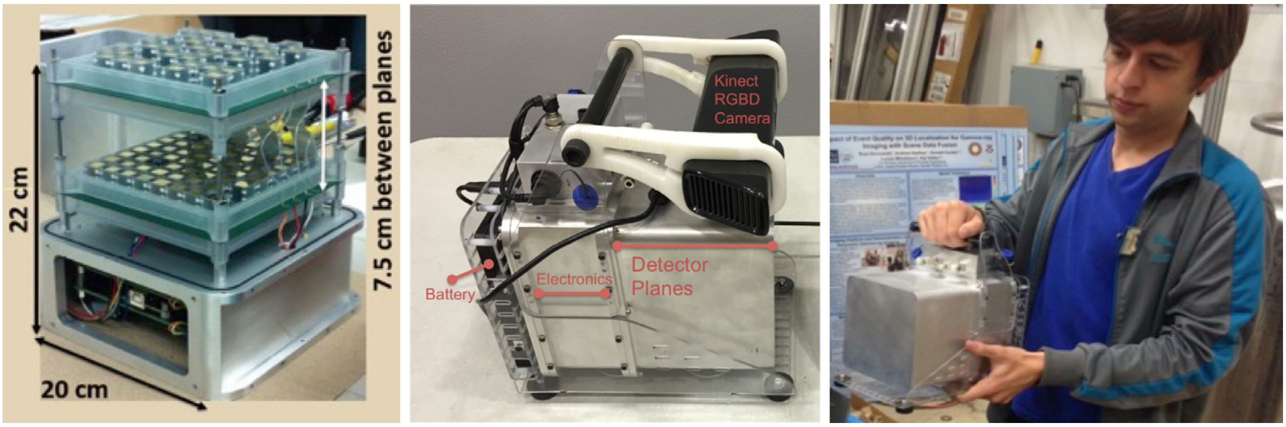

Fig. 4. The High-Efficiency Multimode Imager (HEMI) consists of two layers of coplanar-grid CdZnTe detectors enabling coded aperture and Compton imaging simultaneously. The active mask implementation provides lightweight and high detection efficiency. Even with the Microsoft Kinect sensor, the instrument weighs less than 4.5 kg and is therefore hand-portable.

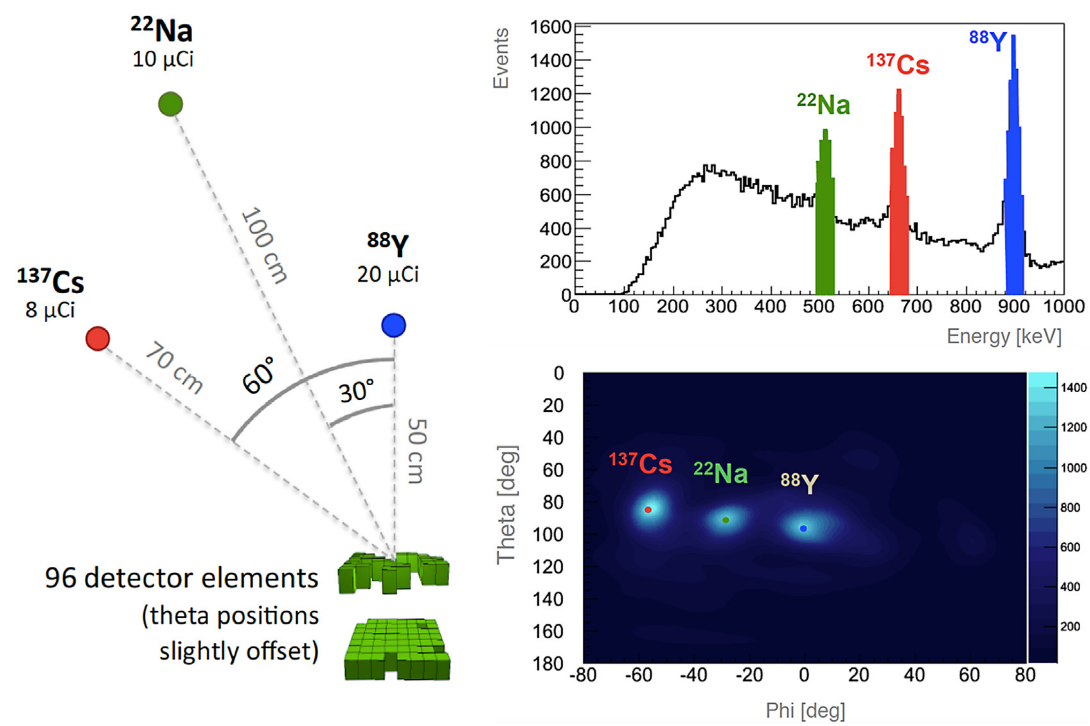

Fig. 5. Demonstration of Compton-scatter based gamma-ray imaging utilizing HEMI. Three point sources (^{22}Na, ^{137}Cs, and ^{88}Y) can be identified via their gamma-ray energy (top right) and localized via Compton imaging (bottom right). The measurement time was about 30 min and the image reconstruction was performed using MLEM with 20 iterations.

capabilities with 96 1 cm^3 CdZnTe (CZT) detectors implemented in coplanar grid (CPG) configuration and arranged in two planes [29–31]. The front plane is equipped with 32 elements arranged in a random pattern providing both the active aperture for the fully populated backplane (for low energies) and a portion of a Compton imaging system, also in combination with the backplane. In the cases presented here, only two-detector events were used for Compton imaging with a minimum lever arm of 2 cm. Since the position resolution is limited to the size of each detector element, the angular resolution, i.e. the ability to separate two point sources, is limited to about 9° for both coded aperture and Compton imaging modalities, the latter at 662 keV. The relative energy resolution of HEMI is about 2% at 662 keV and the intrinsic full-energy efficiency is about 10% at that energy at a distance of 1 m and on axis. About 5% of these events are typically reconstructed to within ±6° in the image.

In the hand-portable format, the HEMI system weighs less than 4.5 kg excluding the external computer that is currently used for running the SLAM algorithm.

Fig. 5 shows the implementation and utilization of the Compton imaging mode for the localization of three point sources. Since HEMI is a gamma-ray spectrometer it can resolve the energies of individual gamma rays to detect and identify specific radio-isotopes and to produce radiation maps associated with them.

Due to its compactness, HEMI can be packaged in an environmental enclosure enabling completely autonomous operation including GPS/IMU, camera, and temperature stabilization on compact aerial platforms. HEMI was mounted on a RMAX Unmanned Aerial System (UAS) provided by the Japan Atomic Energy Agency (JAEA) and flown in contaminated areas in the Fukushima Prefecture in Japan.

In addition, the SDF concept was applied to the Airborne Radiological Enhanced Sensor (ARES) system that was recently developed by

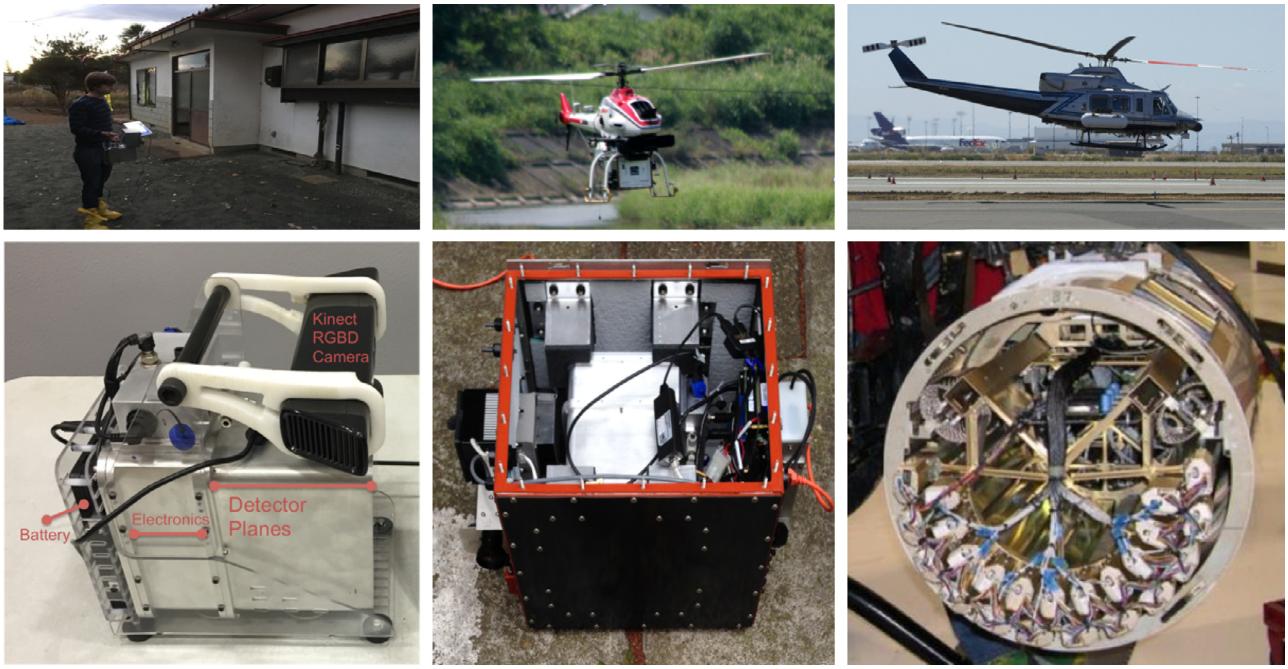

Fig. 6. Examples of packaging and deployments of SDF systems. The HEMI system as deployed in the contaminated area in Fukushima in hand-portable configuration (left) or mounted on an unmanned aerial RMAX helicopter platform (middle). The Airborne Radiological Enhanced Sensor system (right) for the deployment on manned Bell-helicopters consists of identical instruments, one for each of the two pods and each with 46 CsI(Na) detectors arranged in a half-barrel-like geometry.

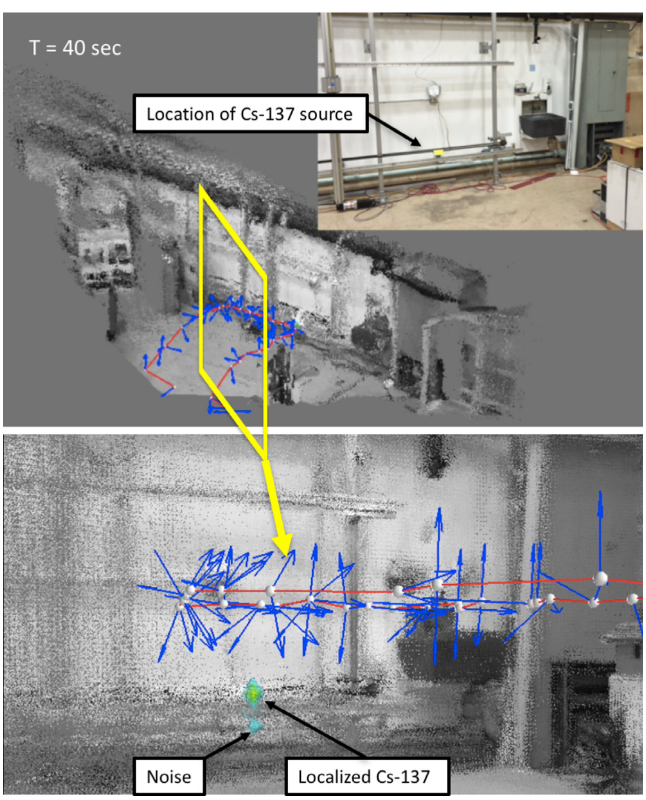

Fig. 7. Detection and 3-D localization of a single Cs-137 point source in our lab. Shown is the final reconstruction from walking around in the scene. The estimation for the Cs-137 source location improves as more data is collected. The blue arrows are the Compton events used in the reconstruction, the line is the path of the detector in the scene and the white circles are the location of the cone vertex. The total measurement time was about 40 s and only 95 events were used for the gamma-ray reconstruction. (For interpretation of the references to color in this figure legend, the reader is referred to the web version of this article.)

the U.S. Domestic Nuclear Detection Office. It consists of two identical instruments, one for each of the external pods mounted on a manned Bell-412 helicopter (Fig. 6). Such helicopters are used by the DOE/NNSA emergency response teams. Each instrument consists of 46 CsI(Na) bars arranged in a aft and fore arrays with 23 detectors and in each, two layers of 11 and 12 crystals mounted in a half-barrel-like geometry (Fig. 8) [32]. Each crystal has the dimensions of $2.5 \times 2.5 \times 40.6$ cm^3 and is read out by a PMT from each end, providing depth-of-interaction information. This arrangement provides good efficiency for a FOV of 170° perpendicular to the flight path while also providing modulation to infer information about the location along this dimension of measured gamma rays. The crystal locations in combination with the depth-of-interaction information can also be used for Compton imaging. In addition, ARES includes seven downward facing high-resolution video cameras, GPS/IMU, a weather station and a radar altimeter. As it was done previously with HEMI in hand-portable or UAS mounted deployments, the visual cameras were used to reconstruct the 3-D scene, which was then fused with the gamma-ray image information.

Other systems have been used as well, such as a cart-mounted gamma-ray imaging system consisting of two high-purity germanium detectors in double-sided strip configuration as used to create the data for Fig. 3. While difficult to transport to other locations, it is useful in the development of advanced concepts such as SDF.

4. Measurements

4.1. Single-source demonstration and benefits of SDF

Fig. 7 illustrates the concept of SDF in our UC Berkeley laboratory, here obtained with the hand-portable High-Efficiency Multimode Imager (HEMI) in combination with a Microsoft Kinect sensor. The combined sensor system was moved freely through the space as indicated by the red line and the reconstructed point cloud and the embedded photograph in the figure. By walking through the 5×8 m^2 space in about 40 s it was possible to detect and localize the Cs-137 source with an activity of 10 μCi in three dimensions as shown in the lower part of the figure. Only 95 events were needed for the reconstruction. With so few events for the image reconstruction, we observe noise as shown in Fig. 7. For comparison and to indicate the gain in the detection speed and resolution by employing SDF with a freely moving gamma-ray imaging system, Fig. 8 shows images obtained with HEMI positioned in the center of the scene and operated statically. The distance between source and instrument was 2.6 m. The two-dimensional images are obtained employing the real-time filtered back-projection reconstruction described in [26]. It takes about 20 min and almost 1000 events to produce an image that allows the accurate location of the source. While the result appears more robust, the spatial resolution is degraded and only providing the two-dimensional location of the source and not the distance. The degradation in spatial resolution is due to the larger distance between the source and the static instrument as compared to the mobile measurement where the majority of the reconstructed events are obtained at closer proximity to the source. This comparison illustrates the advantage of increased speed in the detection and localization of sources by utilizing SDF with a freely moving system and overcoming the $1/r^2$ solid angle loss in radiation flux.

In addition to the increased speed and accuracy in the detection and 3-D localization of radiological materials, several other advantages of SDF are noteworthy: (1) Based on the reconstructed surfaces, objects can be voxelized and sources in these objects localized in 3-D; (2) The scene itself provides important contextual information about the source and its location or use, relevant for the characterization and response to the detection. For example, it can provide means and pathways to minimize risks to the responders and for the consequence management after a release of radiological materials; (3) The full measurement including the scene, time sequences of gamma-ray events, and the path taken can be recorded and replayed later, e.g. for post-verification and re-evaluation.

4.2. Ground-based measurements

HEMI was used in several indoor and outdoor measurement campaigns to further demonstrate SDF, specifically in the localization of multiple sources and in relevant environments. Fig. 9 illustrates the ability to localize three different point sources, which were positioned on top and inside of a cabinet in our lab. The source identification was achieved by measuring the energies of the sources with HEMI. The 3-D source localizations were accomplished by integrating the scene data with the gamma-ray image while moving alongside the cabinet as indicated in the figure. Some artifacts, specifically associated with the Ba-133 and Na-22 sources can be seen and are likely due to backgrounds in the gates of the lower energies of these isotopes. The artifacts can be dealt with in a real search measurement by utilizing the location information that is provided in near real-time to get closer or stay longer at a suspected position to enhance the statistics and clarity of the signal.

This example illustrates a capability of SDF, which is of interest for the assessment and localization of point sources in a lab environment, relevant for a "lost-source" scenario or for the remediation of nuclear facilities. Fig. 10 shows an example of utilizing SDF in emergency response, nuclear safeguards, or homeland security and proliferation detection and search applications with the goal to detect, localize, and identify sources. The enhanced capability for search scenarios, including the localization and identification of radioactive materials and the determination of the potential threat posed by the material is relevant for homeland security, nuclear non-proliferation, and generally the detection of nuclear materials nationally and internationally. In emergency response scenarios it provides additional new means to assess and characterize objects and it contents following a detection by other means, relevant to stabilize or render an object safe.

SDF can also be employed in scenarios associated with distributed sources. It provides fundamentally new capabilities in the monitoring, mapping, and visualization of dispersed radioactive materials after events such as the Dai-ichi nuclear power plant accident or the intentional releases of radiological or nuclear materials in a terrorist attack, or in the remediation and decommissioning of nuclear facilities. The releases of radioactive materials after the Dai-ichi nuclear power plant pose two distinct challenges, the mapping of the radioactive contamination in the environment outside of the nuclear power plant and the assessment of the contamination and fuel debris inside the nuclear facility. The effective mapping of contamination in the environment is critical in guiding the evacuation and resettlement of residents or providing input for calculations to model and predict the evolution and transport of the radioactive materials. In addition, it provides important guidance and verification of decontamination efforts relevant for the decontamination efforts and the safety and well-being of the returning residents. SDF not only provides enormous gains in the speed and accuracy in the mapping and assessment of radioactive materials even in complex environments, it provides new means to visualize the contamination in 3-D of great relevance for experts in the assessment but also for the residents to "see" and better understand the radiation and the associated contamination in and around their homes and neighborhoods. Instead of simple point measurements of dose rates utilizing Geiger counters and noting the dose rate on a sheet of paper while estimating the location of the measurement as it still the state-of-the art procedure, SDF provides the potential for a fully automated registration and full 3-D mapping of the dose-rates in indoor and outdoor environments. In the following, we show two distinct examples to illustrate the power of SDF in the mapping and visualization of contamination in one home in the Fukushima prefecture in Japan.

Fig. 11 shows the results of SDF using HEMI in the mapping of Cs-137 contamination of the outside of a house in Namie-Machi in the Fukushima Prefecture in Japan. This house and its surroundings were contaminated during the Dai-ichi nuclear power plant accident and the house was evacuated. The front of the house was decontaminated by JAEA just before the measurements to ensure safe access. By walking around the house – which took less than five minutes – with the HEMI instrument and contextual sensors it was possible to reconstruct the 3-D model of the house and to fuse the gamma-ray image with the model in 3-D. Since the infrared based structured light of the Microsoft Kinect sensor does not work in direct sunlight, it was replaced with a video camera. The visual imagery was then used to map and reconstruct the scene. Areas with elevated Cs-137 levels can clearly be identified. Specifically the area in the middle of the house on top of a gutter is noteworthy as it shows the highest levels. By closer inspection it was observed that foliage had accumulated on top of the gutter resulting in the increased Cs-137 contamination. In addition, the effectiveness of the decontamination of the front of the house could be confirmed as no Cs-137 was detected there. In contrast, Cs-137 contamination was detected, identified, and localized in the back of the house, which was not decontaminated. These findings indicated several important aspects of SDF: The localization of contamination and hot spots, which require contamination and the verification of decontamination activities.

Fig. 12 shows a bedroom on the first floor of this home as it was mapped with HEMI in combination with the Microsoft Kinect sensor, specifically the structured light sensor to create the point cloud and the visual camera for colorization of the point cloud. Within less than two minutes this room was mapped in 3-D with SDF. A hotspot of Cs-137 activity can be observed in the middle of the ceiling, which is collocated with damage due to the earthquake and leakage of rainwater, which was contaminated with Cs-137 during or briefly after the accident. In addition, Cs-137 can be seen on the walls, floor, and in the mattress on the floor. These observations are consistent with the contaminated rainwater flowing down the walls or dripping to the floor and accumulating in the mattress. As these measurements were performed in December 2015, these images illustrate that important information about the contamination and Cs-137 transport can be gained years after the event happened.

Both examples clearly illustrate the power of SDF employing the hand-portable HEMI system: fast and accurate detection and mapping of radioactive materials in the context of its environment, equivalent with seeing gamma radiation in three dimensions. This technology is relevant for applications ranging from contamination mapping to remediation and decommissioning of nuclear facilities.

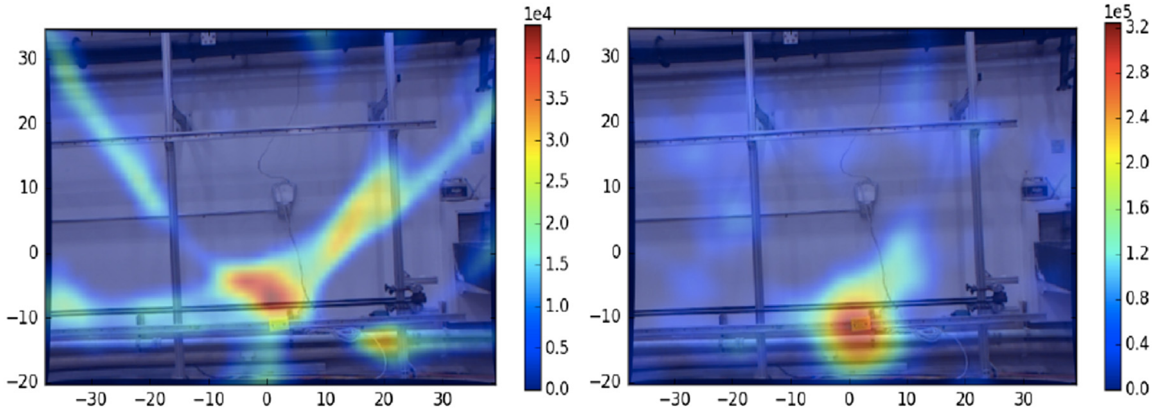

Fig. 8. Illustration of static 2-D Compton images of the Cs-137 source with a visual overlay of the lab scene. The left image shows the image after one minute with 58 events. The right image shows the image after 20 min and 985 events.

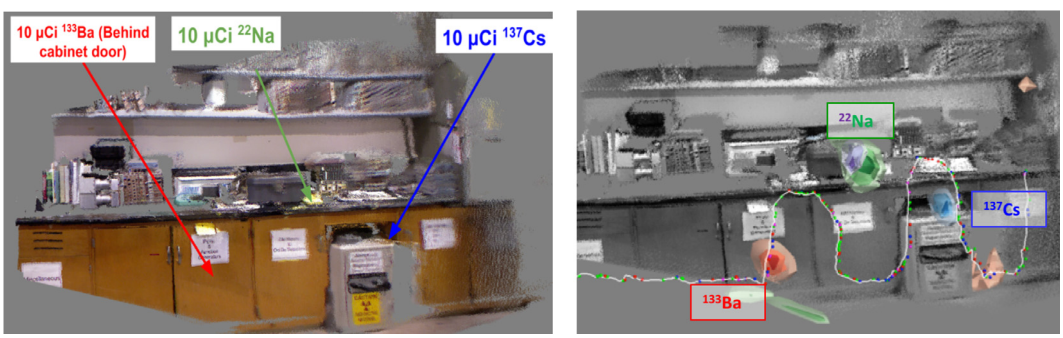

Fig. 9. Detection, identification, and 3-D localization of multiple point sources in a lab environment with the hand-portable HEMI in combination with a Microsoft Kinect sensor and employing SDF. Left: The reconstructed colorized point cloud of the scene with the location of the three point sources. Right: The reconstructed and fused gamma-ray image with the Ba-133 source identified by the energy of 356 keV, the Na-22 source identified by the energies of 511 keV (green) and 1275 keV (purple), and the Cs-137 source by the energy of 662 keV. The white line indicated the reconstructed path of the instrument. The measurement time was less than 1 min. (For interpretation of the references to color in this figure legend, the reader is referred to the web version of this article.)

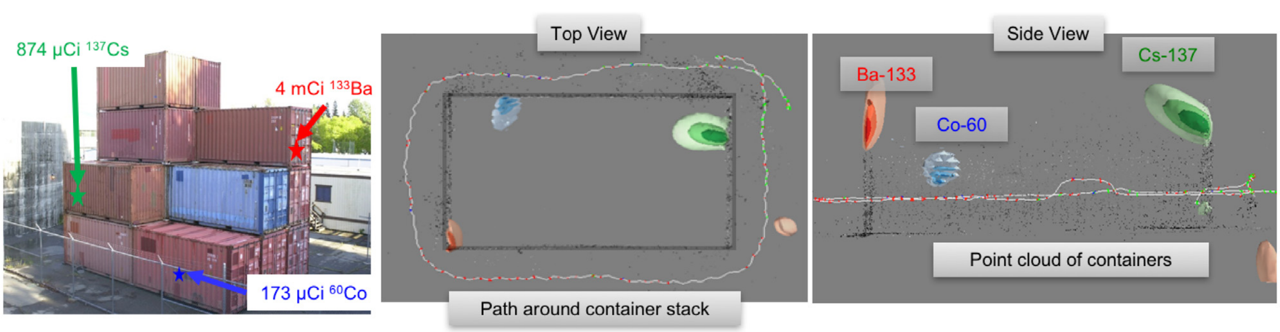

Fig. 10. The detection, identification, and localization of 3 point sources in an outside scene with a stack of cargo shipping containers (left). All three sources were detected and localized in their 3-D locations by employing SDF with HEMI and a visual camera. The visual camera was used to create the point cloud and to estimate the pose of the instrument during the path around the containers as indicated by the white line. The containers were voxelized and the gamma-ray images image reconstructed into the 3-D voxels providing the accurate localizations of the sources.

4.3. Aerial measurements

Scene data fusion cannot only enhance hand-portable or more generally land-based systems, the methods can similarly be applied to aerial systems. Airborne nuclear detection and mapping instruments have several advantages over land-based systems as they can access areas that are otherwise inaccessible, they can map areas much more quickly because they are not hindered by obstacles, their use reduces operator exposure to radiation, and they can reach areas of interest more quickly. For example, radiological assistance teams or first responders to accidental or intentional releases of radiological or nuclear materials are typically on foot to inspect or screen materials or areas using hand-portable instruments. This approach works in many, particularly local incidences, but provides very limited information, particularly for large-scale events associated with extensive damage and contamination. The spatial range for which a foot-borne system is sensitive is typically several meters and operators of such systems have limited access and are exposed to the hazardous environments and contamination. In contrast, aerial systems can overcome these limitations. Currently, in the US there are several fixed and rotary wing manned aerial systems stationed in two locations that can respond and map radiation from high altitudes (at least 300 m for fixed wing aircraft and at least 50 m for helicopters). The purpose of these systems is to support the

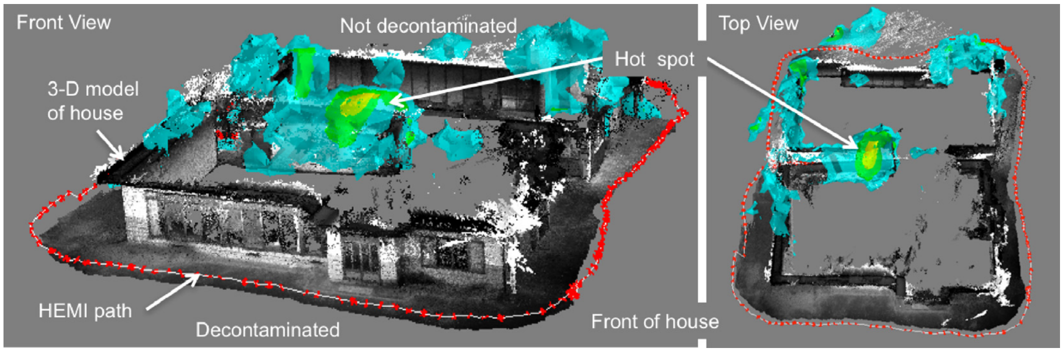

Fig. 11. Reconstructed house and fused gamma-ray image in 3-D. The contour map reflects the reconstructed gamma-ray intensity with a gate on 662 keV associated with Cs-137 contamination on the outside of the house. The highest intensity in the center of the house (which is accessible from the exterior) was found on top of a gutter with accumulated foliage. The dose rate was measured separately to be about 6 μSv/h at 30 cm from the source. There is no Cs-137 detected at the decontaminated front of the house while there is Cs-137 found at the back of the house which was not decontaminated.

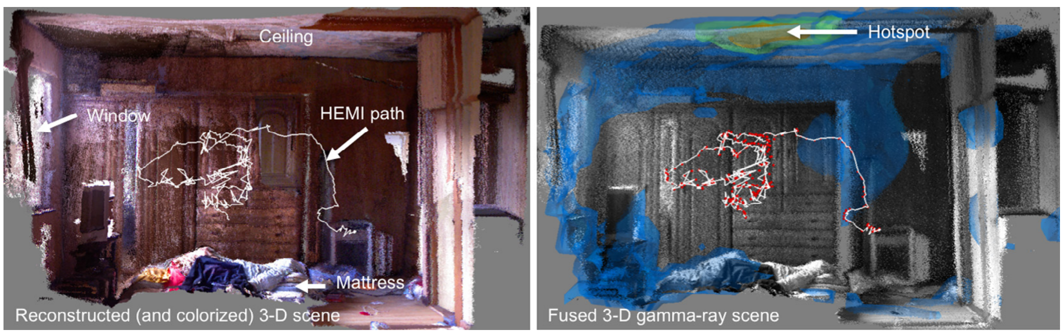

Fig. 12. Reconstruction of a bedroom in the contaminated and evacuated home in Fukushima Prefecture. Left: Colorized point cloud indicating the cluttered environment in this room reflecting the impact of the earthquake and the hurried evacuation of the residents. Right: Fused image showing the reconstructed distribution of Cs-137 in this room. The orange contour on the top points to a leak in the ceiling. Based on this distribution, one can assume that rain water contaminated with Cs-137 leaked through the damaged ceiling and flowed along the walls to the floor ultimately accumulating in the mattress in the middle of the room. (For interpretation of the references to color in this figure legend, the reader is referred to the web version of this article.)

mapping of contamination within a timeframe of several hours to days, particularly to support the consequence management after an event. The ARES system as shown in Fig. 8 was recently developed by the U.S. Domestic Nuclear Detection Office, to enhance not only the nuclear instrumentation but to simultaneously measure contextual information based on high-resolution video cameras and thereby providing the basis for SDF. Fig. 13 shows results of a measurement employing SDF [33]. Buildings were reconstructed in 3-D utilizing the visual imagery and fused with the gamma-ray image information with an energy gate around 662 keV. Two-dimensional visual images are converted to three-dimensional surfaces by employing Structure-from-Motion techniques. Specifically, Scale-Invariant Feature Transform algorithms are being utilized providing the matching of image features and the reconstruction of structures in three dimensions [34].

An intentionally placed Cs-137 point source with an activity of 1.5 mCi was detected and localized in 3-D on top of the building. The presented data were collected in about 8 s in a single over-flight at an elevation of about 50 m above the building rooftop, with a speed of approximately 38 m/s. The obtained resolution was in the order of 1–2 m. Conventional means using localization by proximity typically provide 10's of meters spatial resolution in these scenarios.

In addition to large-scale and manned systems, SDF can be deployed on smaller-scale and unmanned aerial systems (UAS) as well. Fig. 14 illustrates this concept again utilizing HEMI now mounted on a RMAX helicopter as shown in Fig. 8. HEMI is mounted in an environmental enclosure that allows an independent operation of the instruments including a GPS/IMU, video camera, cooling, and control. In addition, it allows the mechanical decoupling of the instruments from the vibrations of the helicopter. Fig. 14 shows results of mapping Cs-137 contamination around a river bed in the evacuated area in the Fukushima Prefecture. Such areas are of particular concern since contamination can change quickly and substantially due to the water flow and changes in water levels and their proximity to residential and populated areas. The area covered in this measurement run is about 100×60 m^2. The data was taken at an elevation of about 10 m with a speed of 1 m/s and a total measurement time of about 25 min. The image on the left shows a radiation map obtained with conventional means by interpolating between counts in the 662 keV energy window associated with Cs-137 as a function of the 2-D position over the ground. Since the flight height is about 10 m, the spatial resolution is in the order of 20 m. In addition, no distances to objects are taking into account in the reconstruction, resulting in artifacts in the activity reconstruction. Utilizing the visual camera and GPS in combination with the Structure-From-Motion concept, we are able to reconstruct the surface in 3-D – as shown in the middle panel of Fig. 14 – and to estimate the 3-D position and orientation of HEMI relative to this surface. The red line reflects the reconstructed flight path over the terrain, with its surface also reconstructed in 3-D. The right panel of Fig. 14 shows a top view of the reconstructed surface, flight, path, and fused gamma-ray image information. As in conventional mapping, the gamma-ray image reconstruction is performed for events with a detected energy of 662 keV. The boundaries of the road and river with less contamination can be clearly distinguished and separated with a resolution of ~1 m, consistent with the achievable angular resolution and altitude of the flight. In addition, the hot spots shown in the conventional map are not visible anymore. These hot spots are due to taller trees, which were just much closer to the radiation detector than its surrounding and therefore leading to the increased count rate. Conventional methods assume just the elevation above ground for the reconstruction, which results in artifacts in these environments where the Cs contamination is

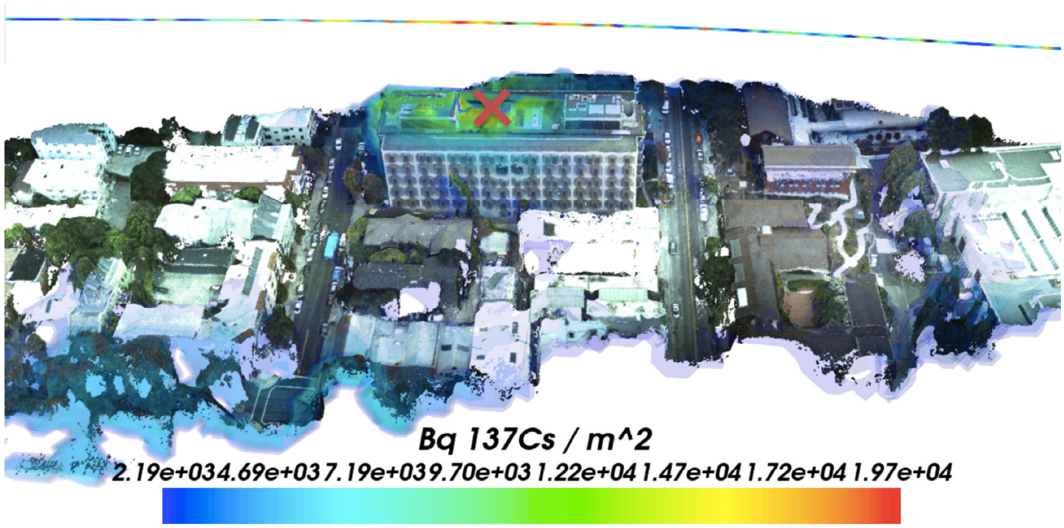

Fig. 13. Reconstruction of a city scene and integrated gamma-ray image in 3-D obtained with the ARES system mounted on a Bell 412 helicopter. A 1.5 mCi Cs-137 point source was located on the roof of the building, as indicated by the red X. MLEM of the 662 keV photopeak from ^{137}Cs was used in the SDF shown. The line on top indicates the flight path of the helicopter and the relative counts measured along the path. (For interpretation of the references to color in this figure legend, the reader is referred to the web version of this article.)

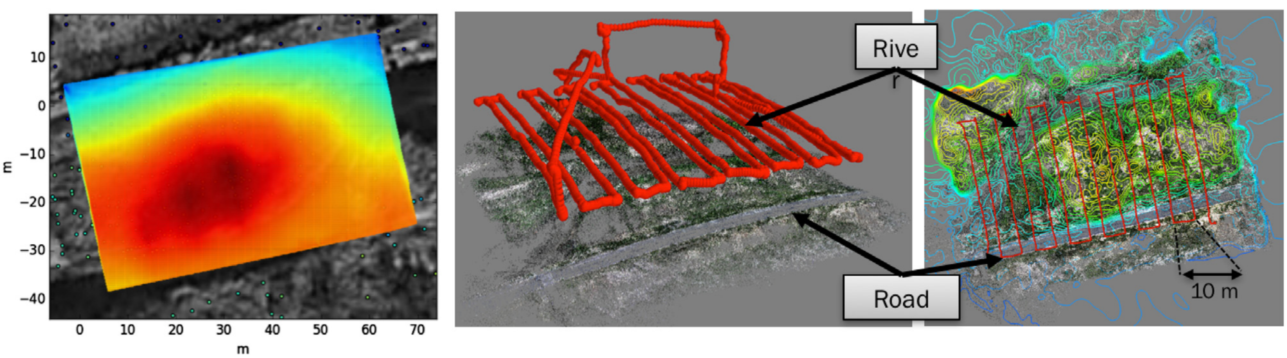

Fig. 14. Results of mapping Cs-137 around a river in the Fukushima Prefecture utilizing HEMI on an unmanned RMAX aerial system. Left: Radiation map obtained with conventional means by interpolating between counts in the 662 keV energy window associated with Cs-137 as a function of the 2-D position over the ground. Middle: Reconstructed 3-D surfaces and reconstructed flight path in 3-D relative to the surface. Right: Top view of the reconstructed surface, flight, path, and fused gamma-ray image information based on the 3-D SDF concept. (For interpretation of the references to color in this figure legend, the reader is referred to the web version of this article.)

not only on or in the ground but deposited on top of or taken up in the vegetation as it can be seen on the left of the figure. Knowledge of the distance between the instrument and the vegetation is necessary for the improved reconstruction of gamma-ray emission intensities.

5. Summary

The Scene-Data Fusion concept was introduced, which provides significant improvements in the effective and accurate detection and mapping of radiological materials relevant for nuclear security and safety. It leverages the enormous advances in sensing and computer vision technologies and combines it with advanced concepts in nuclear detection and imaging. It provides similar means of data fusion and potentially with a similar impact as multi-modality fusion had in medical and biomedical imaging. It combines contextual data of the environment or scene with the radiological data in 3-D and in many cases can be performed in real time. In contrast to medical imaging, the object to be imaged is not well constrained and projections cannot be obtained from a fixed and well-described path. As part of the demonstrated SDF concept, the scene can be reconstructed in 3-D with a freely moving system that can map the scene and estimate the pose of the instrument in real time relative to the scene, which is the prerequisite for the accurate radiation image reconstruction. Not only can the scene and image be reconstructed in 3-D, it can be done accurately and effectively by fusing the radiation with the scene data, e.g. the point cloud. An additional feature is the ability to voxelize objects and to reconstruct the distribution of radiation within these objects also in 3-D. Since the instrument is portable it can also overcome the $1/r^2$ effect and increase the sensitivity in detection over statically deployed detection or imaging systems. SDF has been demonstrated on several land-based and aerial platforms reflecting the fact that this concept is platform independent. The concept has and will have a profound impact in nuclear safety and security ranging from non-proliferation detection to nuclear safeguards and from monitoring of nuclear facilities to contamination mapping, remediation, and decommissioning of nuclear facilities. Finally, in addition to all the quantitative advantages of SDF, it provides new means to “see” radiation in 3-D in the context of its environment. It helps the operator using the instrument, the expert to analyze and re-analyze the measurements, and the layman to address one of the main concerns and fear about radiation, the fact that we cannot sense and see it. Scene Data Fusion brings us a step closer to gamma-ray vision in three dimensions.

Acknowledgments

The work presented here reflects contribution of many scientists and students of the Berkeley Applied Nuclear Physics program. We would like to acknowledge the support from Mark Amman and Paul Luke of LBNL in the development of HEMI. Tatsuo Torii and Yoshiaki Shikaze of JAEA supported the measurements in the Fukushima Prefecture. This work was performed under the auspices of the U.S. Department of Energy by Lawrence Berkeley National Laboratory under Contract DE-AC02-05CH11231. It has been supported by the US Department of Homeland Security, Domestic Nuclear Detection Office, under competitively awarded contract 2011-DN-077-ARI049-03 as well as under Grant Award Numbers ECCS-1140069 and IAA HSHQDC-11-X-00380. In addition, it is based upon work supported by the Department of Energy National Nuclear Security Administration under Award Number(s) DE-NA0000979, Office of Defense Nuclear Nonproliferation Research and Development (DNN R&D), and in collaboration with the Japan Atomic Energy Agency under the Work-For-Others agreement FP00002328. Part of the work has been supported by the Lawrence Berkeley National Laboratories' SBIR program.

References

[1] C.G. Wahl, W.R. Kaye, W. Wang, F. Zhang, J.M. Jaworski, A. King, Y.A. Boucher, Z. He, The Polaris-H imaging spectrometer, Nucl. Instrum. Methods A 784 (2015) 377. http://dx.doi.org/10.1016/j.nima.2014.12.110.

[2] PHDS Co. –Germanium Gamma Ray Imaging Detectors, URL <http://phdsco.com/>.

[3] S. Takeda, A. Harayama, Y. Ichinohe, H. Odaka, S. Watanabe, T. Takahashi, H. Tajima, K. Genba, D. Matsuura, H. Ikebuchi, Y. Kuroda, T. Tomonaka, A portable Si/CdTe Compton camera and its applications to the visualization of radioactive substances, Nucl. Instrum. Methods A 787 (2015) 207. http://dx.doi.org/10.1016/j.nima.2014.11.119.

[4] A. Kishimoto, J. Kataoka, T. Nishiyama, T. Taya, S. Kabuki, Demonstration of three-dimensional imaging based on handheld Compton camera, J. Instrum. 10 (11) (2015) P11001. http://dx.doi.org/10.1088/1748-0221/10/11/P11001.

[5] Y. Sanada, T. Torii, Aerial radiation monitoring around the Fukushima Dai-ichi Nuclear Power Plant using an unmanned helicopter, J. Environ. Radioact. 139 (2015) 294. http://dx.doi.org/10.1016/j.jenvrad.2014.06.027.

[6] P.G. Martina, S. Kwong, N.T. Smithb, Y. Yamashiki, O.D. Paytona, F.S. Russell-Pavier, J.S. Fardoulis, D.A. Richards, T.B. Scott, 3D unmanned aerial vehicle radiation mapping for assessing contaminant distribution and mobility, Int. J. Appl. Earth Obs. Geoinf. 52 (2016) 12.

[7] P.G. Martin, O.D. Payton, J.S. Fardoulis, D.A. Richards, Y. Yamashiki, T.B. Scott, Low altitude unmanned aerial vehicle for characterising remediation effectiveness following the FDNPP accident, J. Environ. Radioact. 151 (2016) 58.

[8] O. Gal, et al., CARTOGAM — a portable gamma camera for remote localization of radioactive sources in nuclear facilities, Nucl. Instrum. Methods A 460 (2001) 138.

[9] O. Gal, et al., Development of a portable gamma camera with coded aperture, Nucl. Instrum. Methods A 565 (2006) 233.

[10] M. Gmar, et al., GAMPIX: a new generation of gamma camera, Nucl. Instrum. Methods A 652 (2011) 638.

[11] K. Amgarou, V. Paradiso, A. Patoz, F. Bonnet, J. Handley, P. Couturier, F. Beckerc, N. Menaaa, A comprehensive experimental characterization of the iPIX gamma imager, J. Instrum. 11 (2016) P08012. http://dx.doi.org/10.1088/1748-0221/11/08/P08012.

[12] K.-P. Ziock, C.B. Boehnen, J.P. Hayward, A.C. Raffo-Caiado, A Mechanically- Cooled, Highly-Portable, HPGe-Based, Coded-Aperture Gamma-Ray Imager, Technical Report, Oak Ridge National Laboratory (ORNL), 2010.

[13] L. Mihailescu, K. Vetter, D. Chivers, Standoff 3D gamma-ray imaging, IEEE Trans. Nucl. Sci. 56 (2) (2009) 479.

[14] CREATEC Co. - N-Visage™ Gamma Image, URL https://www.createc.co.uk/case_study/blue-bear/.

[15] A. Haefner, R. Barnowski, R. Pavlovsky, K. Vetter, Handheld real-time volumetric gamma-ray imaging, Nucl. Instrum. Methods A 857 (2017) 42.

[16] R. Barnowski, A. Haefner, L. Mihailescu, K. Vetter, Nucl. Instrum. Methods A 800 (2015) 65.

[17] K. Vetter, Multi-sensor radiation detection, imaging, and fusion, glenn knoll memoriam issue, Nucl. Instrum. Methods A 805 (2016) 127.

[18] F. Endres, J. Hess, N. Engelhard, J. Sturm, D. Cremers, W. Burgard, IEEE International Conference on Robotics and Automation, ICRA, 2012. p. 1691.

[19] R.W. Todd, J.M. Nightingale, D.B. Everett, A proposed gamma camera, Nature 251 (1974) 132.

[20] V. Schoenfelder, et al., A telescope for soft gamma ray astronomy, Nucl. Instrum. Methods 107 (1973) 385.

[21] J.W. LeBlanc, et al., C-SPRINT: a prototype Compton camera system for low energy gamma ray imaging, IEEE Trans. Nucl. Sci. NS-45 (3) (1998) 943.

[22] S.E. Boggs, W. Coburn, D.M. Smith, et al., Overview of the nuclear Compton telescope, New Astron. Rev. 48 (2004) 251.

[23] E.A. Wulf, B.F. Phlips, et al., Germanium strip detector Compton telescope using three-dimensional readout, IEEE Trans. Nucl. Sci. NS-50 (4) (2003) 1182.

[24] L. Mihailescu, K.M. Vetter, M.T. Burks, E.L. Hull, W.W. Craig, SPEIR: A Ge Compton camera, Nucl. Instrum. Methods A 570 (2007) 89.

[25] K. Vetter, et al., High-sensitivity Compton imaging with position-sensitive Si and Ge detectors, Nucl. Instrum. Methods A 579 (2007) 363.

[26] A. Haefner, D. Gunter, R. Barnowski, K. Vetter, A filtered back-projection algorithm for 4 compton camera data, IEEE Trans. Nucl. Sci. 62 (4) (2015) 1911.

[27] L. Parra, H.H. Barrett, List-mode likelihood: EM algorithm and image quality estimation demonstrated on 2-D PET, IEEE Trans. Med. Imaging 17 (2) (1998) 228.

[28] Microsoft Kinect; https://www.microsoft.com/en-us/download/details.aspx?id=40278.

[29] M. Galloway, A. Zoglauer, M. Amman, S.E. Boggs, P.N. Luke, Simulation and detector response for the high efficiency multimode imager, Nucl. Instrum. Methods A 652 (2011) 641.

[30] M. Amman, P.N. Luke, J.S. Lee, L. Mihailescu, K. Vetter, A. Zoglauer, C.B. Wunderer, M. Galloway, S.E. Boggs, H. Chen, P. Marthandam, S. Awadalla, S. Taherion, G. Bindley, Detector module development for the high efficiency multimode Imager, in: IEEE Nuclear Science Symposium Conference Record, 2009. p. 981, (http://dx.doi.org/10.1109/NSSMIC.2009.5402446).

[31] P. Luke, Unipolar charge sensing with coplanar electrodes application to semiconductor detectors, IEEE Trans. Nucl. Sci. 42 (4) (1995) 207.

[32] B. Quiter, T. Joshi, M. Bandstra, K. Vetter, CsI(Na) detector array characterization for ARES program, IEEE Trans. Nucl. Sci. 63 (2016) 673.

[33] T.H. Joshi, R.J. Cooper, J. Curtis, M. Bandstra, B.R. Cosofret, K. Shokhirev, D. Konno, A comparison of the detection sensitivity of the poisson clutter split and region of interest algorithms on the RadMAP mobile system, IEEE Trans. Nucl. Sci. 63 (2) (2016) 1218.

[34] D.G. Lowe, Distinctive image features from scale-invariant keypoints, Int. J. Comput. Vis. 60 (2004) 91. http://dx.doi.org/10.1023/b:visi.0000029664.99615.94.